Inorganic Chemistry

Article

pubs.acs.org/IC

Particle on a Boron Disk: Ring Currents and Disk Aromaticity in B_{20}^{2-}

Truong Ba Tai,[†] Remco W. A. Havenith,*[,‡] Jos L. Teunissen,[‡] Ahmet R. Dok,[†] Simon D. Hallaert,[†] Minh Tho Nguyen,*[,†] and Arnout Ceulemans*[,†]

[†]Department of Chemistry, University of Leuven, B-3001 Leuven, Belgium

[‡]Theoretical Chemistry, Zernike Institute for Advanced Materials, University of Groningen, Nijenborgh 4, 9747 AG Groningen, The Netherlands

Supporting Information

ABSTRACT: The B_{20}^{2-} cluster is predicted to exhibit a planar sheet-like structure with a circular circumference. Orbital plots and energy correlations demonstrate the close correspondence between the electronic structure of B_{20}^{2-} and the Bessel functions describing the waves of a quantum mechanical particle confined to a disk. The π-band of B_{20}^{2-}, and its B_{19}^{-} congener, contains 12 π-electrons, forming a $(1\sigma)^2(1\pi)^4(1\delta)^4(2\sigma)^2$ configuration, which corresponds to a "*disk aromaticity*" electron count. The analogy not only applies to the π-band, but also extends to the 50 valence σ-electrons. The occupied σ-orbitals are assigned on the basis of radial and angular nodes of the scalar disk waves. The magnetic response of the cluster was examined by Nucleus Independent Chemical Shift (NICS) values and current density calculations based on the ipsocentric model. B_{20}^{2-} is found to exhibit a remarkable inner paratropic current in the σ-channel and an outer diatropic current in the π-channel. The orbital excitations responsible for the antiaromaticity in σ and the disk-aromaticity in π are identified.

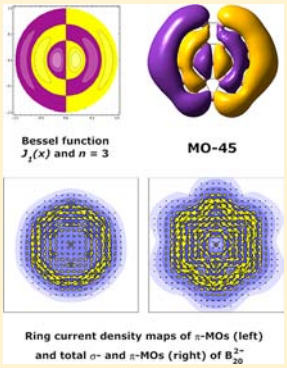

INTRODUCTION

The model of a particle on a ring provides a simple conceptual approach to the electronic structure of annular molecules. The two-dimensional analogue of the ring model is a circular disk model. It is expected to be applicable to planar molecular arrays with a circular shape. Examples may be provided by boron clusters, which can arrange in densely packed disks with nuclearities from 6 to 20. In the present paper we compare the molecular orbitals (MOs) of the largest disk-like cluster, B_{20}^{2-}, to the wave pattern of a particle-on-disk. The results enable us to explain the unusual ring currents in this cluster.

The application of aromaticity concepts to planar boron clusters was first recognized by Fowler and Ugalde, who noted the presence of an aromatic sextet for the B_{13}^{+} planar cation.[1] Double aromaticity, covering both in-plane σ orbitals and out-of-plane π orbitals, was invoked to explain the structure and bonding of B_8 and B_9 wheel structures, for which photoelectron spectra could be observed.[2] Aromatic boron clusters were reviewed as potential new inorganic ligands and building blocks.[3] The aromaticity concept has later been used to design new transition-metal centered monocyclic boron wheel clusters.[4] Deviations from the Hückel model start to appear when larger planar clusters are examined. Huang et al.[5] performed a combined theoretical and experimental investigation on the anionic boron cluster B_{19}^{-}. Their findings showed that B_{19}^{-} exhibits a beautiful planar structure that is composed of two concentric boron rings with one central B-atom. Although this anion has an aromatic character on the basis of negative Nucleus Independent Chemical Shift (NICS) values,[6] its MO picture generally does not follow the Hückel rule of $(4N + 2)$. The anion contains in fact 12 delocalized π electrons. To rationalize this feature, the authors proposed that the anion has a double π-aromaticity corresponding to two concentric delocalized π-electron systems, with six electrons each. In a recent communication, we found that the anionic B_{20}^{-} and B_{20}^{2-} clusters also exhibit polycyclic planar structures, being composed of one outer thirteen-membered ring, one inner six-membered ring, and one central B-atom.[7] The B_{20}^{2-} dianion is also found to be an aromatic system whose MO pattern is similar to that of the B_{19}^{-} anion. We showed that the π-orbital energies and shapes of MOs of B_{20}^{2-}, and also of B_{19}^{-}, match well with those obtained from the simple model of a particle in a circular box. As the twelve valence π-electrons in both systems close a cylindrical shell of a disk, we proposed that both these molecules exhibit *disk aromaticity*. So far this analysis only referred to the 12 delocalized π electrons. In addition the valence shell of B_{20}^{2-} contains 50 σ electrons. We need to examine if these comply with the particle model as well. What are the implications of the σ electron distribution for the disk-aromaticity?

MODEL

The "particle in a one-dimensional linear or circular box" is the simplest example for the solution of the Schrödinger equation, and is widely used in textbooks of elementary quantum chemistry to treat linear and cyclic π-conjugated systems. The particle-on-a-disk model can be considered as a two-dimensional analogue of the particle-on-a-ring problem.[8] It describes a free particle moving on a plane encircled by infinite walls. The

Received: June 24, 2013
Published: September 6, 2013

   dx.doi.org/10.1021/ic401596s | *Inorg. Chem.* 2013, 52, 10595−10600

radius of the disk is denoted by $r = R$. In polar coordinates, the Schrödinger equation for this problem is written as follows

$$-\frac{\hbar^2}{2\mu}\left(\frac{\partial^2}{\partial r^2} + \frac{1}{r}\frac{\partial}{\partial r} + \frac{1}{r^2}\frac{\partial^2}{\partial \varphi^2}\right)\psi(\varphi, r) = E\psi(\varphi, r) \quad (1)$$

where μ is the mass of the particle.

Because of the circular symmetry, the $\psi(\varphi,r)$ can be written as $R(r)\ \Phi(\varphi)$, with $\Phi(\varphi) = 1/(2\pi)^{1/2}\ \exp(im\varphi)$. The cyclic boundary condition requires the angular part to be periodic. As a result the cylindrical quantum number must be integer: $m = 0, \pm 1, \pm 2,...$ Substitution into the Schrödinger equation will give us for the radial part:

$$\frac{\partial^2 R(r)}{\partial r^2} + \frac{1}{r}\frac{\partial R(r)}{\partial r} + \left(k^2 - \frac{m^2}{r^2}\right)R(r) = 0 \quad (2)$$

with $\hbar^2k^2 = 2\mu E$. This equation is known as Bessel's differential equation,[9] and its solutions are the integer Bessel functions $J_m(kr)$. The potential wall at $r = R$ requires the radial function to vanish at the boundary of the box: $J_m(kR) = 0$. The radii that correspond to the zeros of the Bessel function are denoted as $a_{m,n}$. Here n is a radial quantum number that counts the zeros. As k has the dimension of a reciprocal length, the product kR *is dimensionless* and so are the $a_{m,n}$ quantities. They give rise to a quantization of the energy as follows

$$E = \frac{\hbar^2(a_{m,n})^2}{2\mu R^2}, \quad \text{with}$$

$$n = 1, 2, 3, ...; m = 0, \pm 1, \pm 2, \pm 3, ... \quad (3)$$

The rotational quantum numbers are usually denoted by Greek letters: $m = \sigma, \pi, \delta, \phi, \gamma, ...$ States with nonzero values for m will be 2-fold degenerate. The lowest eigenstates in ascending order are 1σ, 1π, 1δ, 2σ, and so on. All roots for n and m up to 5 are listed in Table 1.

Table 1. First Five Roots of the Bessel Functions of the First Kind, $J_m(x)$, with Integer m Ranging from 0 to 5

n	$J_0(x)$	$J_1(x)$	$J_2(x)$	$J_3(x)$	$J_4(x)$	$J_5(x)$
1	2.4048	3.8317	5.1356	6.3802	7.5883	8.7715
2	5.5201	7.0156	8.4172	9.7610	11.0647	12.3386
3	8.6537	10.1735	11.6198	13.0152	14.3725	15.7002
4	11.7915	13.3237	14.7960	16.2235	17.6160	18.9801
5	14.9309	16.4706	17.9598	19.4094	20.8269	22.2178

Note that the only parameter in this treatment is the radius of the circular box. Previously we have shown that this simple model offers an amazingly accurate description of the π-states in the cyclic boron structures.[7] In the present paper we further confront this model with the energies of the in-plane σ-orbitals. Here too the success of the model is remarkable.

COMPUTATIONAL METHODS

Electronic structure calculations are carried out using the Gaussian 03 suite of programs.[10] Geometry optimization and calculation of the harmonic vibrational frequencies are fully performed using density functional theory (DFT) with the hybrid B3LYP functional,[11,12] in conjunction with the 6-311+G(d) basis set.[13,14] The MO shapes of compounds are plotted by using the B3LYP/6-311+G(d) densities. The NICS values are also calculated at this level. Current density maps for B_{20}^{2-} are computed at the DFT (B3LYP) level using the 6-311+G(2d) basis set with GAMESS-UK[15,16] and SYSMO[17] at the *ipsocentric*[18−20] CTOCD-DZ level. The current densities are plotted in a plane $1a_0$ above the B_{20}^{2-} plane. Contour colors denote the modulus and arrows the in-plane projection of the current in the plotting plane. In the plots, counterclockwise (clockwise) circulations imply diatropic (paratropic) currents.

RESULTS

Electronic Structure of B_{20}^{2-}. The B_{20}^{2-} cluster has a closed-shell structure with 62 valence electrons, distributed over 25 in-plane σ-orbitals and 6 out-of-plane π-orbitals. The minimum energy ground state has C_{2v} symmetry. It is highly fluxional with a very soft libration mode of the inner ring with respect to the outer ring. This mode does not change the disk-like shape, and has very little effect on either the electronic structure or the magnetic response. Nearly for all the valence orbitals of σ-type radial and angular disk quantum numbers can be assigned unequivocally on the basis of the orbital plots. Some examples are illustrated in Figure 1. The complete list of orbital plots is provided in the Supporting Information. The assignments form the basis for a comparison of the particle states to the DFT orbital energies. The correlation for the first 15 roots is almost linear. The slope depends only on one parameter, being the radius R. This radius was adjusted to obtain a slope of 45°. The required R-parameter equals 4.966 Å, to be compared with the average cluster radius of 3.4 Å. The effective value thus exceeds the atomic radius by about one bond length. We will come back to this point in the discussion. By replacing the zeros of the Bessel functions into eq 3, the energies (in units of $\hbar^2/2\mu R^2$) of the lowest-lying states of a particle can now be obtained and compared to the DFT orbital energies. The resulting energies (in Hartree), relative to the ground root, are given in Table 2.

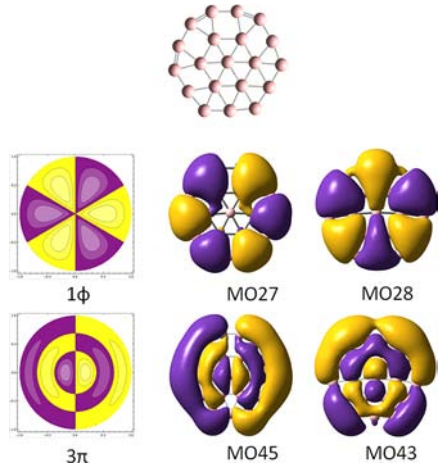

Figure 1. Bessel functions of type 1φ and 3π as compared to corresponding MOs in B_{20}^{2-}.

Figure 2 shows the corresponding correlation plot. From MO39 onward one notes a deviation from a straight line. Inspection of the orbital composition indicates that the lower orbitals have a mixed 2s-$2p_x$,$2p_y$ character, while most of the higher orbitals have a $2p_x$,$2p_y$ character above 85%. The orbital compositions are listed in the Supporting Information. The plots show that these higher orbitals also are characterized by a larger outward extension. This accounts for outer lone-pairs and explains why the slope of the curve is decreasing. Assignments for the top of the σ-band, corresponding to the highest occupied MO (HOMO) and HOMO-1, are not

dx.doi.org/10.1021/ic401596s | Inorg. Chem. 2013, 52, 10595−10600

Table 2. Comparison of DFT σ-Orbital Energies and the Spectrum of a Circular Disk

DFT			particle in circular box	
	label	E (Ha)	label	E (Ha)
MO21	1σ	0.00000	1σ	0
MO22	1π	0.05809	1π	0.0506
MO23	1π	0.06323	1π	0.0506
MO24	1δ	0.12874	1δ	0.1168
MO25	1δ	0.12918	1δ	0.1168
MO26	2σ	0.13554	2σ	0.1400
MO27	1ϕ	0.19890	1ϕ	0.1981
MO28	1ϕ	0.21876	1ϕ	0.1981
MO29	2π	0.23200	2π	0.2464
MO30	2π	0.23231	2π	0.2464
MO31	1γ	0.29339	1γ	0.2938
MO32	1γ	0.29364	1γ	0.2938
MO34	1η	0.38932	2δ	0.3690
MO35	1η	0.39096	2δ	0.3690
MO36	2δ	0.41399	3σ	0.3919
MO37	2δ	0.41458	1η	0.4036
MO38	3σ	0.42544	1η	0.4036
MO39	1ι	0.43841	2ϕ	0.5076
MO40	1ι	0.44201	2ϕ	0.5076
MO43	3π	0.45192	1ι	0.5271
MO44	2ϕ	0.45615	1ι	0.5271
MO45	3π	0.45641	3π	0.5542
MO46	2ϕ	0.52659	3π	0.5542
MO50		0.56601	2γ	0.6616
MO51		0.57009	2γ	0.6616

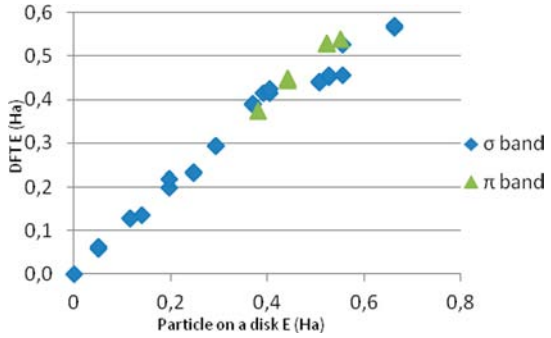

Figure 2. Correlation between DFT orbital energies and particle-on-a-disk spectrum. Shifts were applied to adjust the starting energies of σ- and π-bands. Effective disk radii were determined so as to procure slopes of 45° for both bands.

unequivocal. According to the disk model one would expect a degenerate 2γ pair, while the lowest unoccupied MO (LUMO) and LUMO+1 should be of 3δ character. The orbital plots in Figure 3 of MO50 and MO51 show that both symmetries appear to be mixed. In one direction one observes two radial nodes (n = 3), while in the other only one (n = 2). On the inner ring a δ-type distribution is seen, while on the outer ring there seems to be a γ-sequence of four nodal planes. This orbital composition will be relevant when discussing the magnetic response.

For the π-orbitals, the comparison with the disk model is straightforward. The first orbital is MO33 at 0.3744 Ha. We have introduced this energy as the common starting point of the π-series. The series consists of six orbitals. The optimal correlation was obtained by adjusting the radial size to R = 4.51

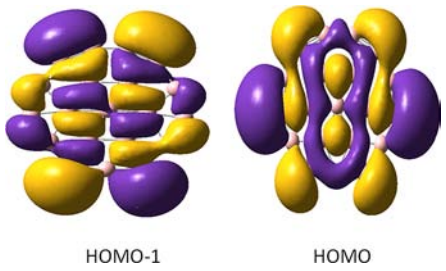

Figure 3. Shapes of the occupied frontier orbitals, showing a mixed disk parentage of type 2γ-3δ.

Å. The extension beyond the atomic radius in this case is only 1.106 as compared to 1.562 for the σ-band. In Table 3 the

Table 3. Comparison of DFT π-Orbital Energies and the Spectrum of a Circular Disk

DFT			particle in circular box	
	label	E (Ha)	label	E (Ha)
MO33	1σ	0.37440	1σ	0.3744
MO41	1π	0.44460	1π	0.4349
MO42	1π	0.44766	1π	0.4349
MO47	1δ	0.52928	1δ	0.5161
MO48	1δ	0.52936	1δ	0.5161
MO49	2σ	0.53794	2σ	0.5443

corrected particle energies are compared to the DFT orbitals. The correlation is also shown in Figure 2. The close match between the shapes of MOs of B_{20}^{2-}, those of B_{19}^{-}, and the disk wave pattern has been demonstrated before.[7] The highest occupied π-MO (HOMO-2) of B_{20}^{2-} contains one nodal plane in the radial direction that is in agreement with the node characteristic of the 2σ-eigenstate of the disk model. In B_{19}^{-} this orbital is the HOMO. According to the classical Hückel rule of $(4N + 2)$ electrons, B_{20}^{2-} should be antiaromatic with N = 3. However, our NICS calculations pointed out that the dianion B_{20}^{2-} exhibits aromatic features.[7] Its NICS value at 1 Å above the center of the ring is −17.4. This is confirmed by calculations of the zz component of the NICS tensor, which reaches −28.7. Further values for different ring positions are supplied in the Supporting Information.

Ring Currents. To gain more insight into the aromaticity of B_{20}^{2-}, we examined its magnetic properties. In the ring current model of magnetic response, aromaticity/antiaromaticity is associated with diatropic/paratropic ring currents that are presented by counterclockwise/clockwise circulations on their maps. The ring currents give a much more detailed picture of aromaticity than the average NICS values at one geometric location.[21,22] Earlier results by Fowler and Gray[23] on the boron wheels B_8^{2-} and B_9^{-} showed that both clusters are characterized by diatropic currents, both in σ and in π. The σ-aromaticity contribution is determined mainly by the closing of the $(2\pi)^4$ in-plane shell. In contrast our results for B_{20}^{2-} show that this extended cluster exhibits π-aromaticity with outer counterclockwise circulation (Figure 4a), but σ-antiaromaticity with inner clockwise circulation (Figure 4b). In the ipsocentric model,[24,25] a virtual excitation from an occupied to an unoccupied MO can result in a contribution to the ring current that is diatropic, paratropic, and null. Accordingly, the diatropic current arises if the product of symmetries of occupied and unoccupied orbitals contains the

dx.doi.org/10.1021/ic401596s | Inorg. Chem. 2013, 52, 10595−10600

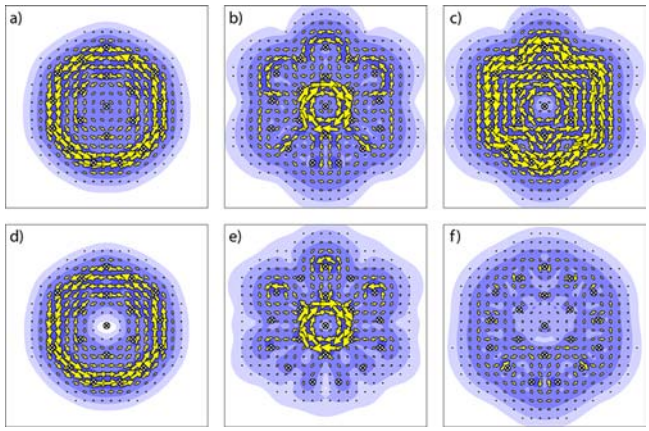

Figure 4. Ring current density maps of (a) π-MOs, (b) σ-MOs, (c) total π- and σ-MOs, (d) HOMO-3 + HOMO-4, (e) HOMO + HOMO-1, and (f) remainder σ (σ − HOMO − HOMO-1) for B_{20}^{2-} (C_{2v}).

in-plane translational symmetry (as the p_x and p_y operators). Oppositely, the paratropic current arises when the product of symmetries of occupied and unoccupied orbitals contains rotational symmetry (as the L_z operator). This rule is relatively simple for planar double-ring structures such as B_{20}^{2-}. If the difference in rotational quantum numbers between the beginning occupied and the final unoccupied orbital is equal to one ($\Delta\Lambda = 1$), it is then diatropic. Otherwise, it is paratropic if this difference is zero ($\Delta\Lambda = 0$). Our maps of excitations for π-HOMOs displayed in Figure 5 clearly show that the main distribution of the total π-aromaticity of the ion B_{20}^{2-} comes from the excitations of HOMO-3 and also HOMO-4 to the unoccupied orbitals LUMO+1 and LUMO+2, respectively. The contribution of these π orbitals show the main features of the π ring current (Figure 4d). The node characteristic of orbitals reveals that both HOMO-3 and HOMO-4 have rotational quantum numbers of 2. This number is increased to 3, corresponding to $\Delta\Lambda = 1$, for unoccupied orbitals LUMO and LUMO+1. The n and m quantum numbers of HOMO-2 are equal to 2 and 0, respectively. These numbers are now increased to $n = 2$ and $m = \pm 1$ for virtual orbital LUMO+2, corresponding to $\Delta\Lambda = 1$. The increase of the rotational quantum number by one unit makes the dianion B_{20}^{2-} π-disk aromatic. A similar observation was noticed for the other fluxional and aromatic species B_{19}^{-}. The node characteristics and energy ordering of the molecular π-orbitals of the B_{19}^{-} are almost the same as those of B_{20}^{2-} (Figure 5). Consequently, the anion B_{19}^{-} is also considered as a disk aromatic system that strictly follows the model proposed. This result is also consistent with the previous report that the B_{19}^{-} exhibits aromatic features on the basis of its negative $NICS_{zz}$ values.[5] The fact that the diatropic current is mainly localized on the outer ring is in line with the spatial distribution of the active LUMO and LUMO+1 virtual orbitals. Further plots are given in the Supporting Information. They show that the remaining π orbitals do not contribute appreciably to the π ring current.

On the other hand the σ-contribution to the density gives rise to a paratropic current on the inner ring. Analysis of the excitations involved clearly shows that the main contribution comes from the transitions between the HOMO and HOMO-1 (Figure 4e) to their virtual counterparts with opposite 2γ-3δ composition. The magnetic interaction thereby connects the xy and $x^2 - y^2$ components of δ, and similarly for the $(xy)(x^2 - y^2)$ and $(x^4 + y^4 - 6x^2y^2)$ components of γ. The other σ orbitals do not contribute significantly to the σ ring current (Figure 4f).

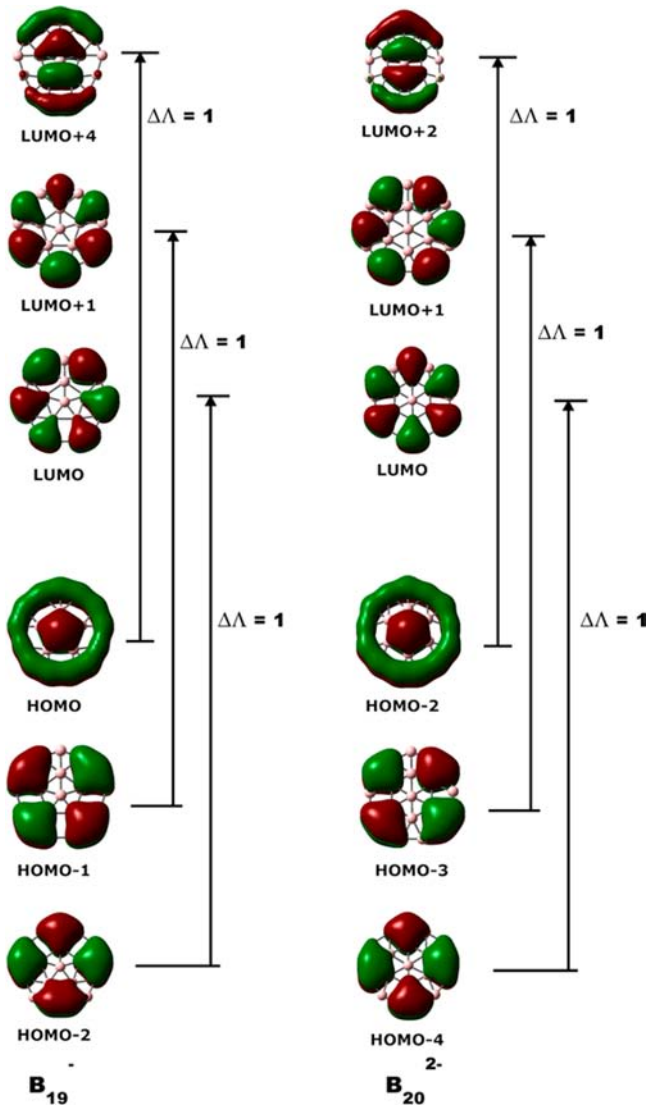

Figure 5. Excitations responsible for diatropic ring currents of B_{19}^{-} and B_{20}^{2-}.

DISCUSSION

The results confirm the close correspondence between the waves for a particle on a disk and the orbitals of planar boron sheets with a circular shape. It is however necessary to distinguish π and σ contributions. The π-orbitals are only based on atomic $2p_z$-functions. These functions do not have in-plane directional properties and recombine to form delocalized MOs. The occupied orbitals of this type have a maximum of only two nodal planes. As a result they show only moderate modulation and are not very susceptible to the details of the atomic structure. This explains why they reflect so well the continuous disk waves and is confirmed by the near degeneracy of the $1\pi_x$ and $1\pi_y$ components, and similarly for the $1\delta_{xy}$ and $1\delta_{x^2-y^2}$ components. This feature also explains why the total π-electron count is similar for clusters with approximately the same size; hence, we find 12 π-electrons both in B_{20}^{2-} and B_{19}^{-}. This also is in line with the theoretical analysis of Sergeeva et al. who identified close analogies between the π-orbitals of 22- and 23-

dx.doi.org/10.1021/ic401596s | Inorg. Chem. 2013, 52, 10595−10600

atom boron clusters and the hydrocarbons anthracene and phenantrene, based on a similar shape.[26] Finally, for the same reason the π shell is not expected to be susceptible to the intramolecular libration mode where the inner ring is rotating inside the outer ring.[27] The analogy has clear limitations though. Since the π-shell only probes the lower part of the spectrum with few nodal characteristics, it cannot reflect the details of the atomic structure, *only the overall size and shape*.

In principle the disk-like characteristics of the σ-sequence are expected to be less prominent. Indeed the in-plane basis orbitals comprise both 2s and $2p_x$, $2p_y$ orbitals. The latter contain a nodal plane which refers to an intrinsic atomic characteristic and is essentially different from an interatomic nodal plane. The resulting directional character of the in-plane 2p orbitals corresponds to a vectorial wave rather than to a scalar wave. In the model of a particle on a spherical surface vectorial and scalar wave are separate solutions of the wave equation,[28] requiring a vector particle model.[29] In principle for the disk a similar distinction should be made.

The orbital compositions show a strong hybridization between the 2s and $2p_x$, $2p_y$ orbitals in the lower region of the spectrum. The slight inflection of the correlation plot from MO39 onward indicates that the 2p contributions become more dominant.

On the whole the orbital plots themselves show such a strong resemblance to a single sequence of *scalar* disk waves, that the distinction between inter- and intra-atomic nodes does not play a role at all. For this reason scalar disk wave assignments can be applied throughout, with the exception of the HOMO-1 and HOMO where the 2γ and 3δ waves are entangled. The fact that the σ-orbitals are much more numerous than the π-orbitals implies that they probe the atomic details of the structure much more closely. This is also reflected in the hybrid nature of the HOMO and HOMO-1. It shows that at the top of the σ-band the MOs deviate considerably from the disk waves which are essentially based on a uniform potential.

The radial fitting parameter indicates that the actual radius of the disk is extended by about one bond length. This is a typical feature of the particle-in-a-box model. The larger extension for the σ-sequence as for the π-sequence reflects the larger extension of the in-plane orbitals because of the presence of the in-plane 2p components.

CONCLUDING REMARKS

To date B_{20}^{2-} is the largest circular boron sheet structure predicted to be an absolute minimum. In this paper we have explored the performance and limitations of the particle-on-a-disk model to explain the electronic structure of this cluster. The model discriminates between π- and σ-bands. There are six occupied π-orbitals which complete a disk shell. As we have indicated before this feature corresponds to the concept of *disk aromaticity*. The in-plane bonding is to be attributed to 25 occupied σ-orbitals. Although they have a mixed s,p-composition, they form a single sequence of scalar disk-like solutions, unlike the spherical analogue which requires the use of tensor harmonics. The radial and angular momenta characteristic of the frontier orbitals are further shown to explain well the remarkable current densities, which are diatropic on the outer ring in π and paratropic on the inner ring in σ.

On the energy scale the σ- and π-bands strongly overlap, and the HOMO and HOMO-1 levels are of σ-type, in contrast to the case of conjugated carbon systems, where the frontier orbitals are always of π-type. So far there does not seem to be a valence bond type theory that can predict for a given planar boron cluster the distribution of the valence electrons over σ- and π-bands.

ASSOCIATED CONTENT

Supporting Information

The coordinates of the 19- and 20-atom boron disks, obtained at the B3LYP/6-311+G(d) level; NICS and $NICS_{zz}$ values calculated at different location in and above the ring; MO plots and atomic orbital composition of all occupied valence orbitals; current density plots of the contributions of the remainder π-orbital space. This material is available free of charge via the Internet at http://pubs.acs.org.

AUTHOR INFORMATION

Corresponding Authors

*E-mail: r.w.a.havenith@rug.nl (R.W.A.H.).
*E-mail: minh.nguyen@chem.kuleuven.be (M.T.N.).
*E-mail: arnout.ceulemans@chem.kuleuven.be (A.C.).

Notes

The authors declare no competing financial interest.

ACKNOWLEDGMENTS

The authors are indebted to the KU Leuven Research Council (GOA and IDO programs). T.B.T. thanks the Arenberg Doctoral School for a scholarship. R.W.A.H. acknowledges Prof. dr. R. Broer (University of Groningen) for fruitful discussions and the Zernike Institute for Advanced Materials ("Dieptestrategie" program) for financial support.

REFERENCES

(1) Fowler, J. E.; Ugalde, J. M. *J. Phys. Chem. A.* **2000**, *104*, 397−403.
(2) Zhai, H.-J.; Alexandrova, A. N.; Birch, K. A.; Bolydyrev, A. I.; Wang, L. S. *Angew. Chem., Int. Ed.* **2003**, *42*, 6004−6008.
(3) Alexandrova, A. N.; Boldyrev, A. I.; Zhai, H.-J.; Wang, L. S. *Coord. Chem. Rev.* **2006**, *250*, 2811−2866.
(4) Romanescu, C.; Galeev, T. R.; Li, W.-L.; Boldyrev, A. I.; Wang, L. S. *Acc. Chem. Res.* **2013**, *46*, 350−358.
(5) Huang, W.; Sergeeva, A. P.; Zhai, H. J.; Averkiev, B. B.; Wang, L. S.; Boldyrev, A. I. *Nat. Chem.* **2010**, *2*, 202−210.
(6) Schleyer, P. v. R.; Maerker, C.; Dransfeld, A.; Jiao, H.; Hommes, N. J. R. v. E. *J. Am. Chem. Soc.* **1996**, *118*, 6317−6318.
(7) Tai, T. B.; Ceulemans, A.; Nguyen, M. T. *Chem.—Eur. J.* **2012**, *18*, 4510−4512.
(8) Robinett, R. W. *Am. J. Phys.* **1996**, *64*, 440.
(9) Steiner, E. *The Chemistry Maths Book*. Oxford University Press: Oxford, U.K., 2008; pp 391−413.
(10) Frisch, M. J. et al. *Gaussian 03*, Revision C.01; Gaussian, Inc.: Wallingford, CT, 2004.
(11) Lee, C.; W. Yang, W.; Parr, R. G. *Phys. Rev. B* **1988**, *37*, 785.
(12) Becke, A. D. *Phys. Rev. A* **1988**, *38*, 3098.
(13) Hariharan, P. C.; Pople, J. A. *Theor. Chim. Acta* **1973**, *28*, 213.
(14) Francl, M. M.; Petro, W. J.; Hehre, W. J.; Binkley, J. S.; Gordon, M. S.; DeFrees, D. J.; Pople, J. A. *J. Chem. Phys.* **1982**, *77*, 3654−3662.
(15) Guest, M. F.; Bush, I. J.; van Dam, H. J. J.; Sherwood, P.; Thomas, J. M. H.; van Lenthe, J. H.; Havenith, R. W. A.; Kendrick, J. *Mol. Phys.* **2005**, *103*, 719−747.
(16) Havenith, R. W. A.; Fowler, P. W. *Chem. Phys. Lett.* **2007**, *449*, 347−353.
(17) Lazzeretti, P.; Zanasi, R. *SYSMO package*; University of Modena: Modena and Reggio Emilia, Italy, 1980.
(18) Lazzeretti, P.; Malagoli, M.; Zanasi, R. *Chem. Phys. Lett.* **1994**, *220*, 299−304.
(19) Steiner, E.; Fowler, P. W. *Chem. Commun.* **2001**, 2220−2221.

(20) Steiner, E.; Fowler, P. W. *J. Phys. Chem. A* **2001**, *105*, 9553−9562.
(21) Pelloni, S.; Lazzeretti, P. *J. Phys. Chem A* **2011**, *115*, 4553−4557.
(22) Pelloni, S.; Manaco, G.; Lazzeretti, P.; Zanasi, R. *Phys. Chem. Chem. Phys.* **2011**, *13*, 20666−20672.
(23) Fowler, P. W.; Gray, B. R. *Inorg. Chem.* **2007**, *46*, 2892−2897.
(24) Keith, T. A.; Bader, R. F. W. *Chem. Phys. Lett.* **1993**, *210*, 223−231.
(25) Coriani, S.; Lazzeretti, P.; Malagoli, M.; Zanasi, R. *Theor. Chim. Acta* **1994**, *89*, 181−192.
(26) Sergeeva, A. P.; Piazza, A. A.; Romanescu, C.; Li, W.-L.; Boldyrev, A. I.; Wang, L. S. *J. Am. Chem. Soc.* **2012**, *134*, 18065.
(27) Zhang, J.; Sergeeva, A. P.; Sparta, M.; Alexandrova, A. N. *Angew. Chem., Int. Ed.* **2012**, *51*, 8512−8515. Jimenez-Halla, J. O. C.; Islas, R.; Heine, T.; Merino, G. *Angew. Chem., Int. Ed.* **2010**, *49*, 5668−5671. Guajardo, G. M.; Sergeeva, A. P.; Boldyrev, A. I.; Heine, T.; Ugalde, J. M.; Merino, G. *Chem. Commun.* **2011**, *47*, 6242−6244.
(28) Stone, A. J. *Mol. Phys.* **1980**, *41*, 1339.
(29) Ceulemans, A.; Mys, G. *Chem. Phys. Lett.* **1994**, *219*, 274.